

## Experiments for Counterflow Flame over a Tsuji Burner

Hsing-Sheng Chai<sup>1\*</sup>, Che-Cheng Chang<sup>2</sup>, and Chiun-Hsun Chen<sup>2</sup>

<sup>1</sup>Department of Air Transport Industry, Aletheia University, New Taipei City 251306, Taiwan

<sup>2</sup>Department of Mechanical Engineering, National Chiao Tung University, HsinChu City 30056, Taiwan

\*Corresponding author E-mail: [au4289@mail.au.edu.tw](mailto:au4289@mail.au.edu.tw)

---

### ABSTRACT

The experiment depicts the counterflow flame stabilization around a Tsuji burner. The parameters of interest are the incoming air flow speed and the ejection velocity of fuel around two Tsuji burners with various fuel ejection area. The flame types and transitions are recorded by a DV recorder. The flame characteristics are categorized into 4 zones (I to IV) for the front half fuel-ejection burner and 2 zones (V and VI) for the full fuel-ejection one. In zones I, II, and III, an envelope flame is around the Tsuji burner at 0.41 m/s initial incoming flow speed condition. Raising the incoming flow speed to a critical one cuts the envelope flame front from the front stagnation region and transfers into a wake flame. The flame colors are different in these zones. In zones IV and V, envelope, wake, lift-off, and late wake flames occur in order with raising incoming flow speed. Fuel can be directly ejected into the lift-off flame in full fuel-ejection burner case, so its survival region is much wider than that in the case of front-half fuel-ejection. In zone VI, the lift-off flame appears to follow directly the envelope flame, and no wake flame is occurred between them. As the incoming flow speed raises further, the wake flame reappears after the lift-off one. Finally, these whole processes are discussed.

**Keywords:** Tsuji burner, counterflow flame, lift-off flame

---

Date of Submission: 02-01-2023

Date of acceptance: 14-01-2023

---

### I. INTRODUCTION

An experimental investigation to identify the lift-off phenomena of a counterflow diffusion flame over a porous cylindrical burner, so-called Tsuji burner, is given in this paper. It is motivated from that the series of experimental studies by Tsuji and Yamaoka (1967, 1969, and 1971) and Tsuji (1982) did not report the lift-off flame phenomena over a porous cylinder, which was identified by Wang (1998) firstly. Although the last work did find the existence of lift-off flame, however, the fuel ejection area was fully covered over the burner surface and the burning was at open air. In addition to these, no satisfactory detailed explanation was given. Therefore, this work establishes an experimental set-up similar to that of Tsuji (1982), as shown in Fig. 1, to investigate the possible existence of the lift-off flame, and determine its mechanism.

Tsuji and Yamaoka (1967, 1969, and 1971) and Tsuji (1982) performed a series of experiments on the counterflow diffusion flame in the forward stagnation region of a porous cylinder. The corresponding extinction limits, aerodynamic effects and the temperature and the stable-species-concentration fields of this flame were considered in detail. These researchers identified two flame extinction limits. Blow-off, due to a large velocity gradient (flame stretch), occurs because of chemical limits on the rate of combustion in the flame zone. Substantial heat losses cause thermal quenching at a low fuel-ejection rate. However, no lift-off flame phenomenon was reported.

The primary configuration in Chen and Weng's numerical study (1990) included a flame over a porous cylinder. That work used the two-dimensional, complete Navier-Stokes momentum, energy, and species equations with one-step finite-rate chemical kinetics. Their parametric studies were based on the Damkohler number ( $Da$ ), a function of inflow velocity, and the dimensionless fuel-ejection rate ( $-f_w$ ), respectively. As  $Da$  was decreased, the envelope, side, and wake flames appeared in that order. However, reducing  $-f_w$  caused the envelope flame directly to become a wake flame, such that no side flame was observed. Also, when a limiting flow velocity was reached, the flame was extinguished completely, without the appearance of lift-off flame.

Zhao et al. (1997) employed USED CARS to measure the temperature distribution in the forward stagnation and wake regions of a methane/air counterflow diffusion flame. A pyrolysis zone of methane is observed on the fuel-rich side of the stagnation region. The temperature of the flame in the wake region is found to exceed that in the stagnation region, implying that some intermediate products are not completely burnt in the latter region.

Dreier et al. (1986) and Sick et al. (1990) took CARS measurements and one-dimensional calculations

to understand the counterflow diffusion flame over a porous cylinder. Their chemical reaction mechanism involved 250 elementary steps (including reverse reactions) and 39 species. They found that discrepancies between experimental and computational results followed from using boundary layer approximations. Apparently, the flow field must be completely represented in two dimensions.

Wang (1998) was the first one who found the lifted flame over a porous cylinder experimentally, but he didn't give a complete discussion about the special phenomena. He conducted experiments to study the flame characteristics using single and dual Tsuji burners, respectively. However, none of the burners were coated on the rear halves of the cylinders. He found that when the fuel-ejection velocity is between 0.3 cm/sec and 0.4 cm/sec, the envelope, wake, and blue lift-off flames appear in that order, as the inflow velocity increases. The blue lift-off flame drops back toward the cylinder and, then, blows off as the velocity increases further. At a fuel-ejection velocity of between 0.4 cm/sec and 0.7 cm/sec, as the inflow velocity increases, envelope, wake, yellow lift-off, blue lift-off, and wake flames appear in sequence. He also identified that the transition velocity of the lift-off flame declines as the fuel-ejection velocity increases. Restated, increasing the fuel-ejection velocity enables the flame to be lifted more easily.

This investigation sets up an apparatus, as shown in Fig. 1, to identify the lift-off flame. Two kinds of porous burners, with different areas through which fuel is ejected, are used here. The map of fuel ejection velocity verses inflow air velocity plots the appearances of the flame to identify their respective existing regimes. The corresponding physical interpretation is also provided.

## II. EXPERIMENTAL APPARATUS

Basically, the experimental setup consists of a wind tunnel and a porous sintered cylindrical burner. Figure 1 depicts the entire experimental structure. The apparatus are described as follows.

### 2.1 Wind Tunnel

The wind tunnel is designed to provide a laminar, uniform oxidizer flow to the porous cylindrical burner, from the surface of which the fuel is ejected. It is open-circuit and orientated vertically upwards. Most of the concepts employed in constructing the wind tunnel follow Yang et al. (1999).

The inlet velocity of the test section is determined by the AMCA 210-85 standard nozzle-method (Air Movement & Control Association Inc., 1985): the volume flow rate is determined and used to deduce the flow velocity. The error in AMCA 210-85 is within 3% when the velocity is between 0.21 m/sec and 3.3m/sec, but becomes 5% when the velocity is under 0.21 m/sec.

The following procedure is adopted to verify the uniformity and stability of the flow velocity in the test section. Four pitot tubes and a fixed static pressure hole are located in front of the burner in the test section (Fig. 2(a)). Change the different connections in the four pitot tubes in order with a fixed static pressure hole under the same inflow velocity for a long enough time. If the pressure differences are approximately equal to each other, then the flow can be regarded as uniform and stable in front of the burner, as depicted in Fig. 2(b).

### 2.2 Porous Sintered Cylindrical Burner

The porous cylindrical burner is comprised of inner and outer parts. The diameter of the inner part is  $20\pm 0.5$  mm, and that of outer part is  $30\pm 0.5$  mm. The outer part is a replaceable piece of porous sintered stainless steel, with  $20\mu\text{m}$  pores and a length of  $40\pm 0.5$  mm. The inner part of the burner is a cylindrical brass rod with internal water-cooling and fuel supply grooves. The outer part is screwed onto the inner part. The cooling device includes a water tank, pump, cooler and connected piping.

The fuel is 99.99% methane ( $\text{CH}_4$ ), and its flow rate is controlled and measured using a digital mass flow controller (MC-2100ENC, Lintec), with a high-performance microprocessor. The fuel ejection velocity is determined by dividing the fuel volume flow rate by the available fuel ejection area over the burner's surface.

### 2.3 Visualization System

A digital video (DCR-TRV50, SONY) is used to visualize and record the flame profiles, such as the envelope, wake, and lift-off flames. A special night-shot function is used to record various flames in a dark laboratory environment. All images, recorded on a cassette tape, are transmitted to a PC for processing and analysis using VideoStudio 4.0 SE Basic (Ulead) software.

### 2.4 Uncertainty Analysis

An uncertainty analysis is carried out to estimate the levels of uncertainty in the experiment. The formulae for evaluating the uncertainty levels in the experiment can be found in many papers, such as those of Kline and McClintock (1953) and Moffat (1982), and in textbooks, such as Holman (1989), Fox and McDonald (1994), and Figliola and Beasley (1995). Accordingly, Table I summarizes the results of uncertainty analysis.

## 2.5 Experimental Repeatability

The procedures for changing the inflow velocities at different fuel ejection velocities were performed three times on each set of data to ensure experimental repeatability, coincidence, and accuracy. The transition velocity, defined as the critical inflow velocity at which an envelope flame is transformed into a wake flame, is crucial in investigating the behaviors of the flame. Table II presents the three measured transition velocities, their mean, and the discrepancy associated with each specified fuel ejection velocity ( $v_w$ ). The discrepancy is defined as the ratio of the absolute difference between the maximum and minimum values of the three data to the average value. Normally, the discrepancies are within an acceptable range (the maximum is 6.82%) and the repeatability is quite good, except at three points, where  $v_w = 1.12$  cm/s, 1.23 cm/s, and 1.68 cm/s. These points are found to be located in the neighborhood of the two demarcation lines, which are between regions I ( $v_w = 0.9 \sim 1.12$  cm/s) and II ( $v_w = 1.23 \sim 1.57$  cm/s), and regions II and III ( $v_w = 1.68 \sim 2.8$  cm/s), respectively, as depicted in Fig. 4. The discrepancies will inevitably be large at these critical points. However, they are below 20%.

## III. RESULTS AND DISCUSSION

The combustion experiments adopt three parameters to observe the flame behaviors behind a porous cylindrical burner. They are the inflow air velocity ( $U_{in}$ ) and the fuel ejection velocity ( $v_w$ ) under two burners with different fuel ejection areas ( $S$ ), respectively. The burner with the forward half fuel-ejection area is defined as  $S=180^\circ$ , whereas the one with the full fuel-ejection area as  $S=360^\circ$ . Several temperature-resistant layers are coated onto the rear half of the  $S=180^\circ$  burner to prevent fuel ejection into the wake region. Restated, the burner is exactly the same as the Tsuji burner. The  $S=360^\circ$  burner, similar to that used by Wang (1998), ejects fuel into the airflow from the entire cylinder. The velocity of the incoming air ranges from 0.21 m/s to 4.0 m/s. The fuel ejection velocity is from 0.9 to 3.14 cm/s for the  $S=180^\circ$  burner, and from 1.01 to 1.68 cm/s for an  $S=360^\circ$  burner.

### 3.1 $S=180^\circ$ Burner

#### 3.1.1 Flame Behaviors without Lift-off

Figure 3 graphically defines the flame stand-off distance, flame thickness, attached angle of the wake flame, flame length and flame lift-off height. These definitions are used to characterize the behaviors of the flames. The flame stand-off distance and flame thickness are defined in the forward stagnation region of the envelope flame, whereas the flame length is the distance measured from the rear stagnation point of the cylindrical burner to the downstream point of reattachment of the flame onto the line of symmetry. Table III summarizes the data corresponding to these definitions at several specific points, which are grouped into four regions described in Fig. 4.

Figure 4 depicts the flame configuration map as functions of inflow and fuel ejection velocities. Each point, which is a mean value of three measured data, as in Table II, on the curve is obtained by adjusting the inflow velocity gradually at a given fuel ejection velocity to obtain the specific flame configuration. The curves can be divided into four regions according to the observed features of the flames. Each region basically includes an envelope, wake, and lift-off flames or extinction. However, extinction may not be observed in all regions because of the limits on the maximum inflow velocity achievable by the wind tunnel.

In Region I, the fuel ejection velocity is between 0.9 and 1.12 cm/s. If the fuel ejection velocity is below 0.9 cm/s at an initial inflow velocity of 0.41 m/s, then the flame is found to be unstable and cannot exist because of the quenching effect of the burner wall. The envelope flames are blue and the subsequent wake flames have the same color, implying that the combustion is a fuel-lean burning.

Figure 5 shows the sequence of flames as the inflow velocity ( $U_{in}$ ) changes from 0.41 to 2.06 m/s under a fixed fuel ejection velocity of  $v_w = 1.12$  cm/s. At  $U_{in} = 0.41$  m/s, a blue envelope diffusion flame is stabilized 1.7 mm in front of the cylinder surface in the forward stagnation region. The flame is approximately 1.7 mm thick and 2D long (Fig. 5 (a) and Table III (a)). As  $U_{in}$  increases to 0.51 m/s, the flame stand-off distance declines to 0.8 mm and the flame length is increased to 2.7D (Fig. 5 (b) and Table III (a)). However, the thickness of the flame is almost invariant. An increase in inflow velocity ( $U_{in}$ ) indicates an increase of the flame stretch effect. When  $U_{in}$  is increased to 0.66 m/s, the flame front breaks from the forward stagnation region. It retreats along the cylinder surface until a balance condition is reached, then, the flame front can be stabilized on the rear part of the cylinder. This type of flame is defined as a wake flame (Fig. 5 (c)). Notably, the wake flame front is ahead of the rear stagnation point in the stream-wise direction. Increasing the incoming flow velocity reduces the rate of the chemical reaction in the flame front, enhancing the flame stretch effect. This effect opens up the envelope flame. The ejected fuel is mixed with the incoming oxidizer to yield a flammable mixture because the envelope flame is blown off from the forward stagnation region. The mixture then flows downstream and is subsequently ignited by the hot gas that recirculates behind the cylinder to initiate a reaction that forms the

wake flame. The air and fuel are mixed before this mixture enters the reaction zone because the flame front is away from the porous section and no fuel is ejected from the rear surface of the cylinder. Also, the mixture has time to diffuse to some extent. Consequently, the flame front becomes flat and broadened. The wake flame is completely blue, implying that the mixture is in the fuel-lean region. Gradually increasing the inflow velocity shortens the flame and increases the attached angle (Figs. 5 (c)-(e) and Table III (a)). When the inflow velocity exceeds 2.43 m/s, the flame is completely extinguished from the rear of the cylinder.

The flame patterns in regions II ( $v_w$  from 1.23 to 1.57 cm/s) and III ( $v_w$  from 1.68 to 2.8 cm/s), shown in Fig. 4, are the same as those in region I. The variations in flame stand-off distance, flame thickness, attached angle of the wake flame, and flame length with inflow velocity exhibit the same trend (Tables III (b) and (c)). The major difference is in the color of the flames. For example, at a fuel ejection velocity of 1.23 cm/s, the blue envelope flame occurs when the inflow velocity is below 0.76 m/s. Increasing the inflow velocity to 0.76 m/s converts the envelope flame into a wake flame, whose flame front exhibits premixed flame characteristics and whose downstream part displays the features of a diffusion flame. The downstream diffusion flame zone is separated into an inner luminous yellow zone and an outer blue zone (Fig. 6 (c)). The appearance of the inner yellow zone due to soot production reveals that combustion in the wake flame front and the part of the preceding diffusion flame do not consume all the fuel, and that the excess fuel allows the burning downstream to be fuel-rich on the fuel side. When the inflow velocity increases to 1.04 m/s, the oxidizer supply rate increases and mixing improves. Therefore, the combustion is more complete upstream and the entire wake flame is blue (Figs. 6 (e)-(g)).

The difference between regions II and III is that the downstream wake region of the envelope flame in region III is yellow, as illustrated in Figs. 7 (a) and (b). This color indicates that the blowing rate of fuel is so great, especially in the lower inflow velocity regime, that some fuel is not completely burnt out but is convected downstream to cause local burning under fuel-rich conditions (Figs. 7 (a)-(b)).

The above experimental observation can be summarized briefly. At a given fuel ejection velocity, the flame stand-off distance declines and the flame length increases as the inflow velocity increases, but the thickness of the envelope flame is almost constant. The attached angle of a wake flame increases and the flame length decreases as the inflow velocity increases. For a fixed inflow velocity, the flame stand-off distance, flame thickness, and flame length of the envelope flame increase with the fuel ejection velocity.

### 3.1.2 Appearance of Lift-Off Flame

Performing the same procedure as in the previous three regions reveals the phenomenon of flame lift-off in region IV, where the fuel ejection velocity is between 2.91 and 3.14 cm/s.

For example, when the fuel ejection velocity equals 3.02 cm/s, an envelope flame with a yellow tail appears when the inflow velocity is 0.41 m/s (Fig. 8 (a)) because much unreacted fuel is carried downstream, leading to fuel-rich burning there. The corresponding flame stand-off distance is 2mm, as presented in Table III (d). Continuously increasing the inflow velocity to 1.00 m/s reduces the flame stand-off distance to 0.8 mm; the flame thickness remains almost constant. The downstream flame becomes longer and extends beyond the test section and into the exhaust part of the wind tunnel because the increased air supply intensifies the combustion. Consequently, no flame length data are available in these cases. At  $U_{in} = 1.39$  m/s, the flame front is suddenly blown off from the forward stagnation region, resulting in a wake flame with an attached angle of  $118^\circ$ . A fixed inflow velocity is maintained for a period. Then, the flame starts to lift away from the rear surface of the cylinder, as shown in Fig. 8 (e). Figure 8 (e) includes ten pictures taken at different times at a fixed inflow velocity of  $U_{in} = 1.39$  m/s and a fuel ejection velocity of  $v_w = 3.02$  cm/s. These pictures reveal that the flame is turbulent with a slightly back-and-forth oscillation. Eventually, the flame drops back to the surface of the cylinder and is converted into a wake flame (called a late wake flame) again, whose attached angle is also maintained at  $118^\circ$ . After such a wake flame is stabilized, increasing  $U_{in}$  slightly to 1.43 m/sec does not alter its configuration, and no flame lift-off occurs. The similar behavior is retained up to  $U_{in} = 3.00$  m/s. See Table III (d).

In summary, as the inflow velocity increases, the envelope, wake, lift-off, and late wake flame appear in order in this region. However, the existing inflow velocity regime of the lift-off flame is quite narrow for a given fuel ejection velocity, as shown in Fig. 8.

## 3.2 S=360° Burner

In this section, the fuel ejection area completely covers the cylinder surface rather than just the front half, as considered in the preceding section. The test procedures are exactly the same as those for the S=180° burner. Figure 9, like Fig. 4, presents a flame configuration map as functions of inflow and fuel ejection velocities. However, the figure consists of only two regions, regions V and VI.

In region V ( $v_w = 1.01$  to 1.34 cm/s), the case of fuel ejection velocity,  $v_w = 1.23$  cm/s, is selected to illustrate the behaviors of the flame. Figure 10 displays corresponding photographs of each flame with various inflow

velocities. The envelope flames with the yellow tail, depicted in Figs. 10 (a) and (b), exist when the inflow velocity is below 0.8m/s. The fuel on the downstream side is not expected to mix well with the air since the fuel is supplied through the whole surface. Consequently, combustion at the downstream tail is by fuel-rich burning. The flame stand-off distance declines as the inflow velocity increases, and the flame thickness remains almost constant (Table IV (a)). The combustion becomes more intense as the air supply rate is increased, lengthening the flame tail and causing it to extend into the exhaust. As in Table III (d), no flame length data are available.

The wake flame appears when the velocity equals 0.8m/s (Fig. 10 (c)). From Table IV (a), the attached angle also increases with inflow velocity ( $101^\circ$  for  $U_{in} = 0.8$  m/s and  $108^\circ$  for  $U_{in} = 1.0$  m/s).

The lift-off flame commences to appear when the inflow velocity reaches 1.05 m/s. The base of the lift-off flame, as shown in Fig. 10 (e-1), can stay for much longer above the cylinder surface than that in region IV of Fig. 4. Consequently, the lift-off height can be clearly measured as 2.5mm (Table IV (a)). The height then oscillates for a short period without a specific frequency (Figs. 10 (e-2) to (e-6)) and finally stabilizes (Fig. 10 (e-7)) at a constant value. The downstream flame includes an inner yellow zone surrounded by a blue zone.

The above flame behaviors are retained as the inflow velocity is increased up to 1.21 m/s. Below this value, the lift-off height increases (Table IV (a)) and the corresponding oscillation frequency increases with the inflow velocity. At  $U_{in} = 1.21$  m/s, the inner yellow zone disappears, and the flame is entirely blue (Fig. 10 (f)).

When  $U_{in}$  exceeds 1.21 m/s, both the lift-off height and the oscillation frequency decline gradually as the inflow velocity increases. When  $U_{in}$  reaches 1.63 m/s, the lift-off flame front drops back to the cylinder again and becomes a late wake flame. Further increasing the inflow velocity does not make the lift-off flame reappear.

The cases of  $S=180^\circ$  and  $S=360^\circ$  burners with  $v_w = 1.23$  cm/sec are compared. The latter one has twice the fuel ejection rate of the former one. Therefore, the downstream wake is fuel-rich burning. However, the forward conditions are the same for both burners. Tables III (b) and IV (a) reveal that the features of envelope flames and the critical velocity at which a wake flame occurs are almost the same in both cases, implying that the downstream influence is negligible in the low inflow velocity regime. However, the attached angle of the wake flame is larger in the latter case, implying that the downstream fuel ejection in the rear of the cylindrical burner more strongly influences the wake flame and leads to the appearance of the lift-off flame.

The main difference between region VI (Fig. 9), where  $v_w = 1.4$  to 1.68 cm/s, and region V is that the lift-off flame appears directly after the envelope flame in that region. Restated, no wake flame is observed between the envelope and the lift-off flames. However, the late wake flame still follows the lift-off flame, as illustrated in Fig. 11, which plots variations in the flame configuration as a function of the inflow velocity at a fixed fuel ejection velocity of 1.4 cm/s. The envelope flame with a yellow tail is presented when the inflow velocity is below 1.06 m/s (Figs. 11 (a)-(c)). The flame stand-off distance falls as the inflow velocity increases, but the flame thickness remains almost constant (Table IV (b)). When the inflow velocity exceeds 1.06 m/s, the envelope flame front is broken up, and directly becomes lift-off flame over the rear surface of the cylinder without any wake flame appearing, as in region VI. Thereafter, the process and the variation of lift-off flame are similar to those in region V. When the inflow velocity increases to 1.24 m/s, the lift-off flame turns into completely blue. The lift-off flame again drops back to the cylinder as the inflow velocity increases to 1.63 m/s.

As shown in Fig. 9, another discrepancy between regions V and VI is that the critical velocity for transforming into the lift-off flame in region V declines as the fuel ejection velocity increases, but region VI exhibits an opposite trend. However, a careful examination of the demarcation line between the envelope and the lift-off flames in region VI reveals that it seems to be extended from the line between the envelope and the wake flames in region V. Figure 4 verifies this behavior, revealing that the critical inflow velocity at which the envelope flame is transformed into the wake flame increases with the fuel ejection velocity.

### 3.3 Explanation of Lift-off Flame Behavior

The above observation indicates that the lift-off flame eventually appears irrespective of whether full or half cylinder fuel ejection is used. The stabilization of a wake flame is well known to depend strongly on the existence of a vortex. As the inflow velocity increases, the attached angle of the wake flame also increases, moving the two flame fronts closer together. Accordingly, the high pressures generated in these two reaction zones (or flame fronts) depress the vortices and eventually destroy them. The lift-off flame then appears. Apparently, the lift-off flame is a premixed flame, in which the fuel and air are mixed upstream. The position of the lift-off flame front depends on the balance between the speed of the flame (that propagates toward the rear surface of the cylinder) and the velocity of the local fresh mixture that flows in the direction of the air flow. However, the lift-off flame oscillates with no predictable frequency. It is because the lift-off flame is turbulent; therefore, the surface of the flame front is wrinkled, continuously changing the balance position. Also, the unavoidable disturbance in the flow field may contribute to the flame oscillations.

From Table IV, the lift-off height increases with the inflow velocity. When the height is sufficiently large, the

flame front is further away from the cylinder's surface, and the vortices are regenerated behind the cylinder. Then, the somewhat unstable lift-off flame front is drawn back by the recirculation flow to become a wake flame again (late wake flame).

The supplied fuel can be directly ejected into the lift-off flame in the full fuel-ejection burner. Therefore, its survival domain is much larger than that of the front half fuel-ejection burner.

### 3.4 Comparisons with Other Studies

The dimensions of Tsuji and Yamaoka's test section (1967, 1969, and 1971) were 18x12x3 cm<sup>3</sup> and the burner diameters were 1.5, 3.0, 4.5, and 6.0 cm; the burners were 3 cm long. The fuels used were propane, city gas, and methane. They focused on the flame behaviors in the forward stagnation region of the cylinder and the blow-off mechanisms that convert envelope flames into wake flames as the inflow velocity increased. However, they did not continue to increase further the inflow velocity to generate the lift-off flame, which is emphasized in this work.

Table V compares the critical non-dimensional fuel ejection rate ( $-f_w=(v_w/U_{in})*(R_c/2)^{1/2}$ ) at each specific flame stretch rate ( $2U_{in}/R$ ). Recall that the viscosity ( $\nu$ ) in Reynolds number ( $Re=(U_{in}R)/\nu$ ) depends strongly on temperature. Tsuji (1982) did not mention his selected value of viscosity. Thus, this study deduces this value from the available data in his paper.

Table V indicates that the critical value of  $-f_w$  for blow-off in this work is always a little less than that obtained by Tsuji (1982). The difference declines as the flame stretch rate increases. The possible reasons for the discrepancies are as follows. The burner and the test section in this work are longer and larger than those used by Tsuji (1982). The controller of the mass flow rate of the supplied methane used here is digital and has a microprocessor. It should be much more precise than an analogue one, especially in the low flow-rate regime. As stated previously, the value of viscosity ( $\nu$ ) may also contribute to the discrepancies.

Wang (1998) used a 4 cm long uncoated burner ( $S=360^\circ$ ) with a diameter of 0.96 cm and LPG as fuel. The fuel ejection velocity was from 0.15 to 1.25 cm/s, and the inflow velocity was up to 5.7 m/s. Although the burner dimensions, fuel, and burning environment used in this study differ from those in the last reference, the decline in the critical velocity of transformation into the lift-off flame with an increase of fuel ejection velocity (region V in Fig. 9), is exactly the same in both studies. Also, the flame configurations and the order of their appearance in the fuel ejection velocity range of 0.3 to 0.7 cm/s considered by Wang (1998) are the same as those in region V of Fig. 9 in this paper. When the fuel ejection velocity exceeds 0.7 cm/s in Wang (1998), the trend in the variation is similar to that in the left half of region VI in Fig. 9 in this work. However, Wang (1998) did not further extend the fuel ejection velocity to the right part of region VI in Fig. 9.

## IV. CONCLUSIONS

Flame characteristics and flame lift-off phenomena behind porous cylinders are investigated experimentally. The experimental apparatus consist of a wind tunnel and a porous sintered cylindrical burner. A digital video, fixed at an appropriate position, records the various flame profiles.

Parametric studies are conducted by changing the inflow velocity ( $U_{in}$ ) and the fuel ejection velocity ( $v_w$ ), using two kinds of burners ( $S=180^\circ$  and  $360^\circ$ ), respectively. For  $S=180^\circ$ , the flame patterns are separated into four regions (I-IV), whereas for  $S=360^\circ$ , they are separated into two regions (V and VI) given by inflow velocity ( $U_{in}$ ) versus fuel ejection velocity ( $v_w$ ). In regions I, II, and III, the envelope diffusion flame is generated around the porous cylinder at an initial inflow velocity of 0.41 m/s. For a fixed fuel ejection velocity, the flame stand-off distance decreases and the flame length increases as the inflow velocity increases, due to the enhanced flame stretch effect. The thickness of the envelope flame is almost constant. Increasing the inflow velocity to a critical value causes the envelope flame front to be blown off and transformed into a wake flame. The flame is shortened and flame attached angle increased as inflow velocity increases. The major difference among these three regions is the color of the flames.

In region IV, the envelope flame turns into a wake flame as the inflow velocity increases. Maintaining the same inflow velocity for a short period enables the flame to be lifted away from the rear surface of the cylinder. A lift-off height can be maintained over a porous cylinder because of the balance between the speed of the flame toward the rear surface and the velocity of the locally fresh mixture in the air flow direction. In the experiment, back-and-forth oscillations of the turbulent lift-off flame are observed because the local balance position is changed continuously by the wrinkling of the flame surface. When the inflow velocity exceeds the critical value, the vortices show up again, and the flame lift-off height gradually declines. Finally, the lift-off flame is drawn back to form a wake flame (late wake flame) again.

In the full fuel-ejection case ( $S=360^\circ$ ), the transformation from the envelope to the wake flame in region V is similar to that in the front half cylinder fuel-ejection case ( $S=180^\circ$ ). However, the fuel ejected from the rear surface cannot mix well with air, resulting in fuel-rich burning in the downstream tail. The lift-off flame is generated as the inflow velocity increases further. The base of the lift-off flame can stay longer above

the surface of the cylinder than that in region IV.

In region VI, no wake flame is observed between the envelope and lift-off flames. Another difference between regions V and VI is that the critical velocity at which the lift-off flame in region V is transformed decreased as the fuel ejection velocity increased. The trend is opposite to that in region VI. The fuel supply can be directly ejected into the lift-off flame in the case of full cylinder fuel-ejection; consequently, the survival domain is much larger than that in the front half cylinder fuel-ejection.

## NOMENCLATURE

a	Length of cross-sectional area of the test section
A	Cross-sectional area of the test section
b	Width of the cross-sectional area of the test section
$D_i$	Inner diameter of the cylinder
$D_o$	Outer diameter of the cylinder
$-f_w$	Nondimensional fuel-ejection rate
H	Flame lift-off height
L	Burner length
$\bar{P}$	Pressure
Q	Volume flow rate
R	Radius of the cylinder
$R_e$	Reynolds number
S	Fuel-ejection area
T	Temperature
t	Time
$U_{in}$	Inflow (air) velocity
$v_w$	Fuel-ejection velocity
$\nu$	Kinematic viscosity
$\rho_{air}$	Density of air

## References

- [1]. Chen, C. H. and Weng, F. B., "Flame Stabilization and Blowoff over a Porous Cylinder," *Combustion Science and Technology*, Vol. 73, pp. 427-446 (1990).
- [2]. Dreier, T., Lange, B., Wolfrum, J., Zahn, M., Behrendt, F., and Warnatz, J., "Comparison of CARS Measurements and Calculations of the Structure of Laminar Methane-air Counterflow Diffusion Flames," *Ber. Bunsenges. Phys. Chem.*, Vol. 90, pp. 1010-1015 (1986).
- [3]. Figliola, R. S. and Beasley, D. E., *Theory and Design for Mechanical Measurements*, 2<sup>nd</sup> Ed., John Wiley and Sons, Canada (1995).
- [4]. Fox, R. W. and McDonald, A. T., *Introduction to Fluid Mechanics*, John Wiley and Sons, Canada (1994).
- [5]. Holman, J. P., *Experimental Methods for Engineers*, 5th Ed., McGraw-Hill, New York (1989).
- [6]. Kline, S. J. and McClintock, F. A., "Describing Uncertainties in Single-Sample Experiments," *Mechanical Engineering*, Vol. 75, pp. 3-8 (1953).
- [7]. Moffat, R. J., "Contributions to the Theory of Single-Sample Uncertainty Analysis," *Journal of Fluid Engineering*, Vol. 104, pp. 50-260 (1982).
- [8]. Sick, V., Arnold, A., Diebel, E., Dreier, T., Ketterle, W., Lange, B., Wolfrum, J., Thiele, K. U., Behrendt, F., and Warnatz, J., "Two-dimensional Laser Diagnostics and Modeling of Counterflow Diffusion Flames," *Twenty-third Symposium (International) on Combustion*, The Combustion Institute, Pittsburgh, pp. 495-501 (1990).
- [9]. Tsuji, H. and Yamaoka, I., "The Counterflow Diffusion Flame in the Forward Stagnation Region of a Porous Cylinder," *Eleventh Symposium (International) on Combustion*, The Combustion Institute, Pittsburgh, pp. 979 (1967).
- [10]. Tsuji, H. and Yamaoka, I., "The Structure of Counterflow Diffusion Flame in the Forward Stagnation Region of a Porous Cylinder," *Twelfth Symposium (International) on Combustion*, The Combustion Institute, Pittsburgh, pp. 997 (1969).
- [11]. Tsuji, H. and Yamaoka, I., "Structure Analysis of Counterflow Diffusion Flames in the Forward Stagnation Region of a Porous Cylinder," *Thirteenth Symposium (International) on Combustion*, The Combustion Institute, Pittsburgh, pp. 723 (1971).
- [12]. Tsuji, H., "Counterflow Diffusion Flame," *Progress in Energy and Combustion Science*, Vol. 8, pp. 93 (1982).
- [13]. Wang, J. Y., "The Effect of Interaction Between Two Porous Flame Mechanism With Nitrogen Ejector," M. S. Thesis, Department of Mechanical Engineering, National Taiwan University, Taipei, Taiwan (1998).
- [14]. Yang, J. C., Donnelly, M. K., Prive, N. C., and Grosshandler, W. L., "Dispersed Liquid Agent Fire Suppression Screen Apparatus," NISTIR 6319, National Institute of Standards and Technology, U. S. A. (1999).
- [15]. Zhao, J., Li, C., and Yang, S., "Measurements of Temperature Distribution in a Counterflow Diffusion Flame by USED CARS," *Laser Technology*, Vol. 21, No. 4, pp. 218 (1997).

Table I Summary of uncertainty analysis

Parameters	Uncertainty
$D_i, D_o, L, a, b$	$\pm 0.5$ mm
$A$	$\pm 1.267\%$
$A_{Burner}$	$\pm 2.084\%$
$V$	$\pm 0.09\%$
$\rho_{air}$	$\pm 0.201\%$
$\bar{T}$	$\pm 0.5$ °C
$\bar{P}$	$\pm 1$ torr
$Q_{air}$	$\pm 2.2\%$
$Q_{fuel}$	$\pm 1\%$
$U_{in}$	$\pm 2.54\%$
$v_w$	$\pm 2.31\%$
$R_e$	$\pm 3.04\%$

Table II Experimental repeatability

Fuel ejection velocity (cm/s)	1 <sup>st</sup> measured value (m/s)	2 <sup>nd</sup> measured value (m/s)	3 <sup>rd</sup> measured value (m/s)	Average value (m/s)	Discrepancy (%)
0.9	0.58	0.55	0.56	0.56	5.33
1.01	0.6	0.56	0.60	0.59	6.82
1.12	0.7	0.6	0.71	0.67	16.42
1.23	0.72	0.65	0.73	0.70	11.43
1.34	0.76	0.75	0.76	0.76	1.32
1.4	0.78	0.77	0.8	0.78	3.83
1.46	0.81	0.79	0.83	0.81	4.94
1.57	0.85	0.82	0.85	0.84	3.57
1.68	0.95	0.84	1.00	0.93	17.20
1.79	0.98	1.01	1.02	1.00	3.99
1.9	1.03	1.04	1.04	1.04	0.96
2.02	1.06	1.05	1.08	1.06	2.82
2.13	1.09	1.07	1.10	1.09	2.76
2.24	1.12	1.09	1.14	1.12	4.48
2.35	1.15	1.13	1.17	1.15	3.48
2.46	1.21	1.16	1.21	1.20	4.19
2.58	1.25	1.22	1.24	1.24	2.43
2.69	1.27	1.25	1.26	1.26	1.59
2.8	1.29	1.28	1.31	1.29	2.32

Table III Characteristics of each kind of flame for S=180°

(a)  $v_w = 1.12$  cm/s

Inflow velocity (m/s)	Stand-off distance (mm)	Flame thickness (mm) or Attached angle	Flame length (D=diameter of cylinder)	Flame type
0.41	1.7	1.7mm	2D	Blue envelope
0.51	0.8	1.7mm	2.7D	Blue envelope
0.66		100°	2.4D	Blue wake
1.00		105°	1.6D	Blue wake
2.06		118°	0.4D	Blue wake

(b)  $v_w = 1.23$  cm/s

Inflow velocity (m/s)	Stand-off distance (mm)	Flame thickness (mm) or Attached angle	Flame length (D=diameter of cylinder)	Flame type
0.41	1.7	2mm	2.1D	Blue envelope
0.62	0.9	2mm	2.6D	Blue envelope
0.76		100°	3.5D	Yellow wake
0.89		102°	3.2D	Yellow wake
1.04		105°	2.3D	Blue wake
1.28		110°	1.1D	Blue wake
2.35		120°	0.2D	Blue wake

(c)  $v_w = 2.46$  cm/s

Inflow velocity (m/s)	Stand-off distance (mm)	Flame thickness (mm) or Attached angle	Flame length (D=diameter of cylinder)	Flame type
0.41	1.9	2mm	5.8D	Yellow envelope
1.0	0.8	2mm	6D	Yellow envelope
1.2		102°	6.2D	Yellow wake
1.25		104°	5.2D	Blue wake
1.58		118°	1.7D	Blue wake
3.10		118°	1D	Blue wake

(d)  $v_w = 3.02$  cm/s

Inflow velocity (m/s)	Stand-off distance (mm)	Flame thickness (mm)	Attached angle or Flame lift-off height (H, mm)	Flame type
0.41	2.0	2.4		Yellow envelope
0.62	1.5	2.4		Yellow envelope
0.71	1.1	2.3		Yellow envelope
1.00	0.8	2.3		Yellow envelope
1.39			118°, 3mm	Lift-off flame after wake flame
1.43			124°	Blue wake
3.00			123°	Blue wake

Table IV Characteristics of each kind of flame for S=360°

(a)  $v_w = 1.23$  cm/s

Inflow velocity (m/s)	Stand-off distance (mm)	Flame thickness (mm) or Attached angle	Flame lift-off height (H, mm) or Attached angle	Flame type
0.41	1.7	2mm		Yellow envelope
0.51	1.0	2mm		Yellow envelope
0.8		101°		Yellow wake flame
1.0		108°		Yellow wake flame
1.05			2.5mm	Yellow lift-off flame
1.21			5mm	Blue lift-off flame
1.63			125°	Late wake flame

(b)  $v_w = 1.4$  cm/s

Inflow velocity (m/s)	Stand-off distance (mm)	Flame thickness (mm)	Flame lift-off height (H, mm)	Flame type
0.41	1.7	2.1		Yellow envelope
0.51	1.1	2.1		Yellow envelope
0.84	1.0	2.0		Yellow envelope
1.06			2mm	Yellow lift-off flame
1.24			6mm	Blue lift-off flame
1.63			130°	Late wake flame

Table V Comparisons with Tsuji's flame blow-off study (1982)

Flame stretch rate (sec <sup>-1</sup> )	Present study's $-f_w$	Tsuji's study's $-f_w$ (1982)	Difference (%)
141.33	0.1307	0.1565	16.49
145.33	0.1359	0.1581	14.04
149.33	0.1410	0.1597	11.71
153.33	0.1460	0.1613	9.49
160	0.1496	0.164	8.78
165.33	0.1543	0.1661	7.10
168	0.1596	0.1672	4.55
172	0.1642	0.1688	2.73

$$\text{Flame stretch rate} = \frac{2U_{in}}{R}$$

$$\text{Nondimensional fuel-ejection rate, } -f = \left( \frac{v_w}{U_{in}} \right) \sqrt{\frac{Re}{2}}, \quad Re = \frac{U_{in} R}{\nu}$$

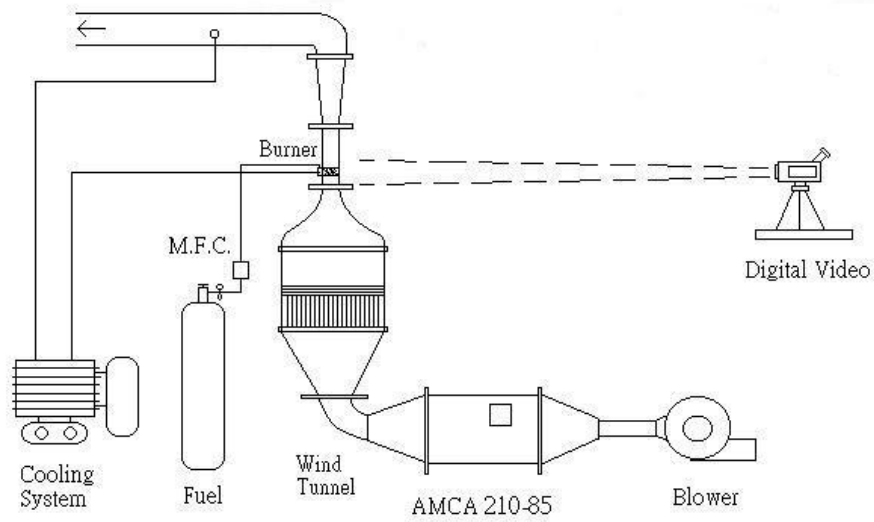
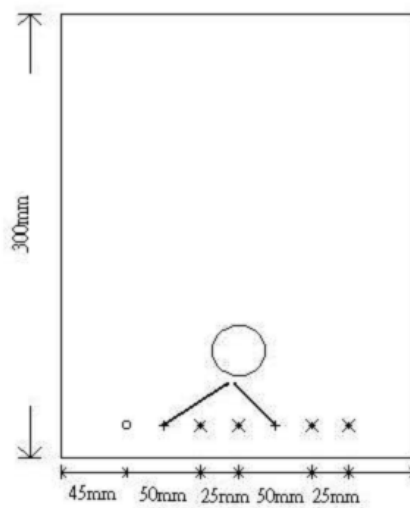
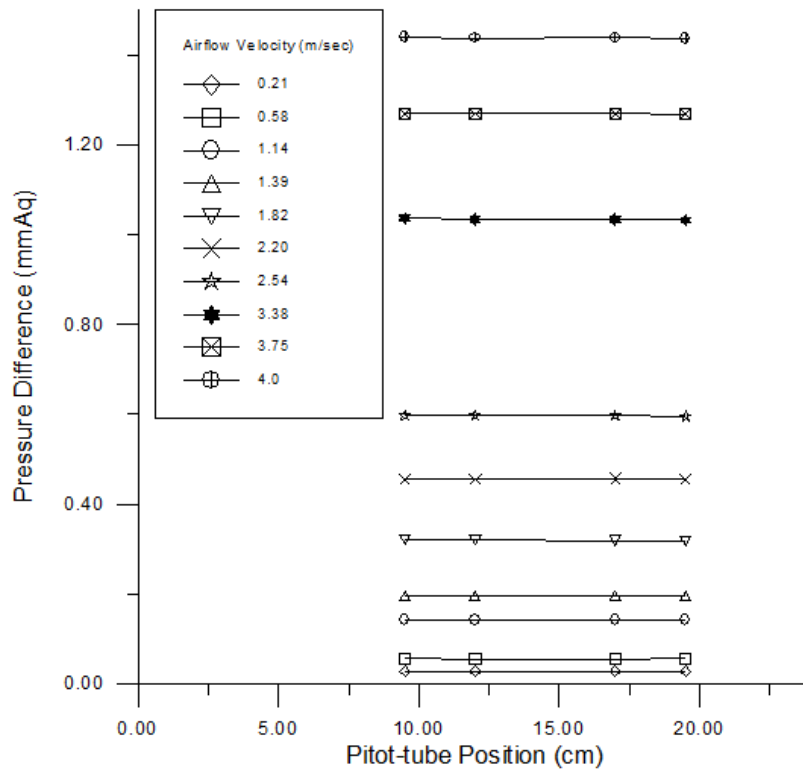


FIGURE 1 Schematic drawing of overall experimental system

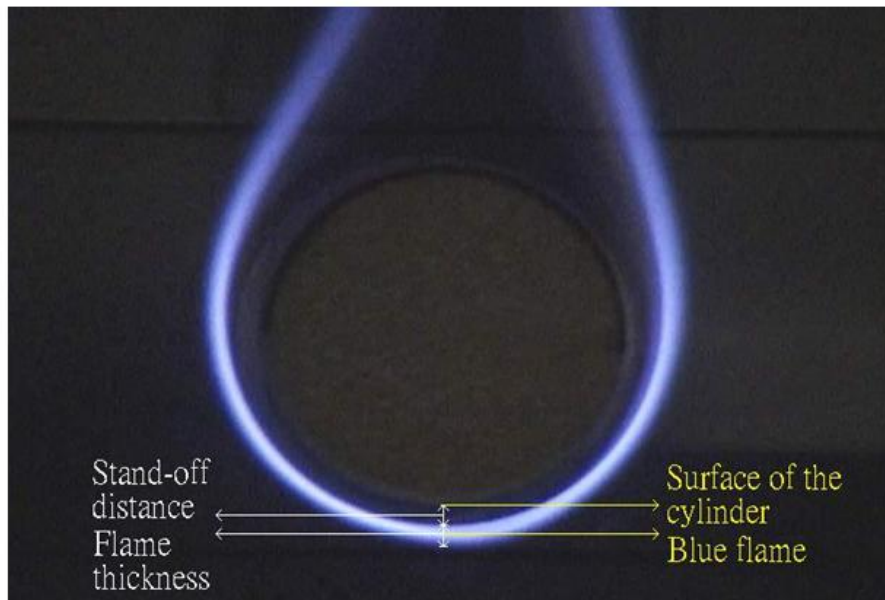


(a)



(b)

FIGURE 2 (a) The position of pitot tube in the test section (b) Pressure difference at various positions in the test section



(a) Flame stand-off distance and flame thickness

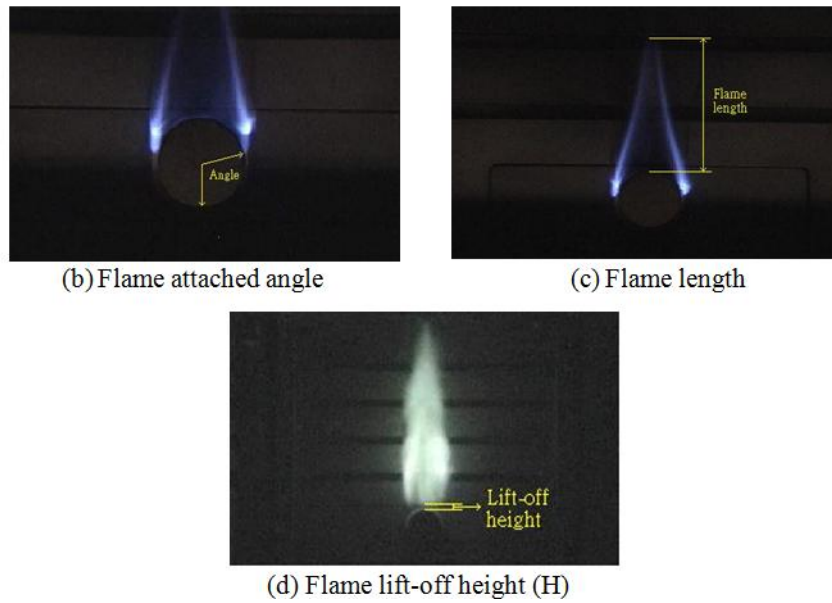


FIGURE 3 Definitions of flame stand-off distance, flame thickness, flame attached angle, flame length, and flame lift-off height for each kind of flame

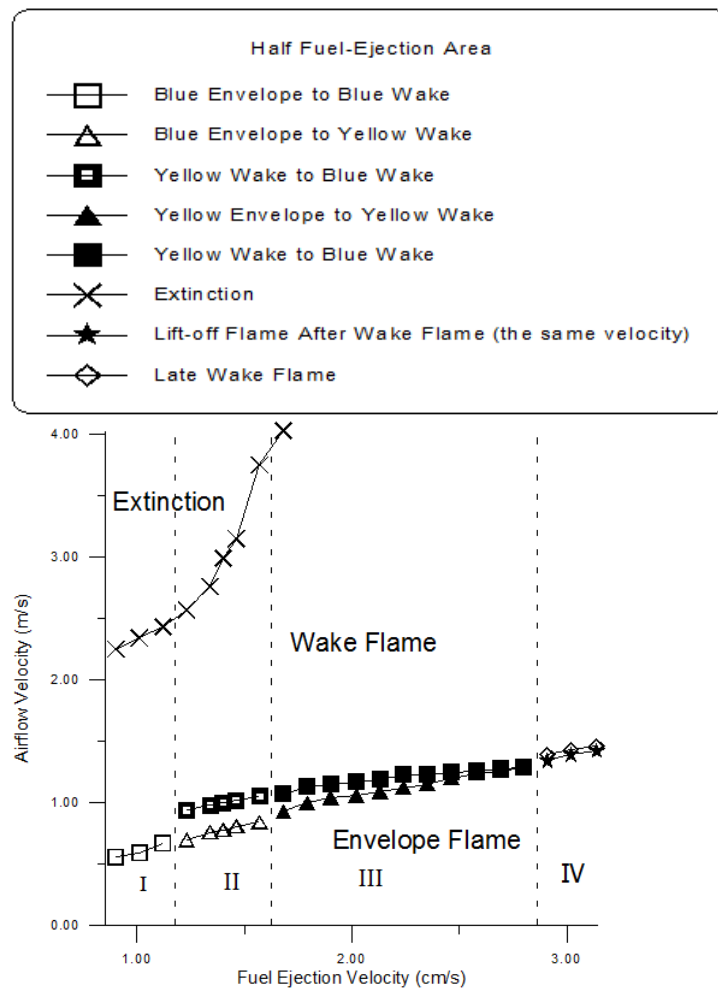


FIGURE 4 Various flame stabilization regions over a burner ( $S=180^\circ$ )

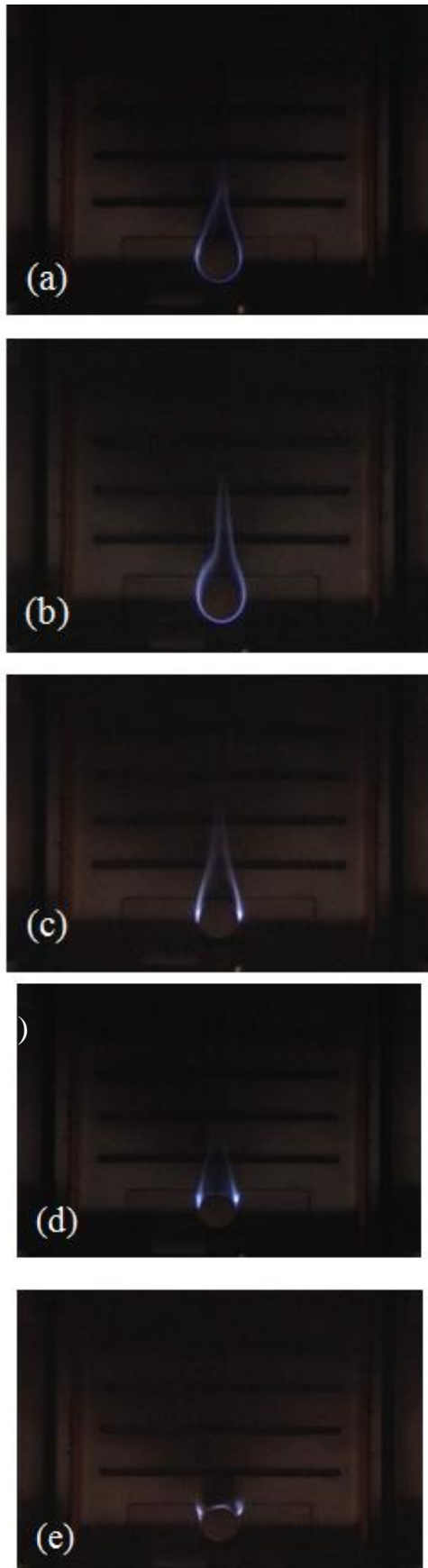


FIGURE 5 Series of flame configurations as a function of inflow velocity ( $v_w = 1.12\text{cm/s}$  and  $S = 180^\circ$ ), (a)  $U_{in} = 0.41\text{m/s}$ , (b)  $U_{in} = 0.51\text{m/s}$ , (c)  $U_{in} = 0.66\text{m/s}$ , (d)  $U_{in} = 1.00\text{m/s}$ , and (e)  $U_{in} = 2.06\text{ m/s}$

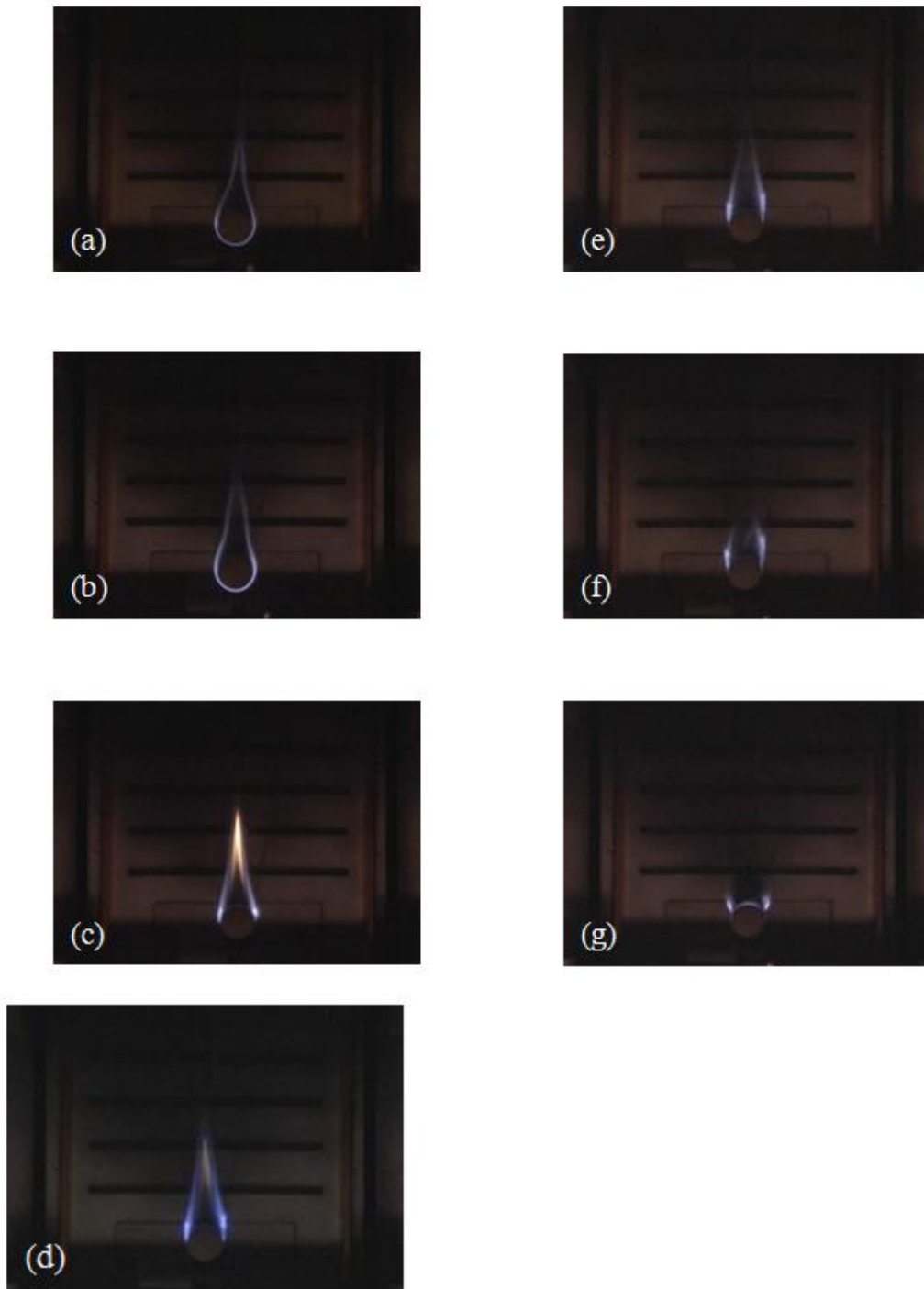


FIGURE 6 Series of flame configurations as a function of inflow velocity ( $v_w = 1.23\text{cm/s}$  and  $S = 180^\circ$ ), (a)  $U_{in} = 0.41\text{m/s}$ , (b)  $U_{in} = 0.62\text{m/s}$ , (c)  $U_{in} = 0.76\text{m/s}$ , (d)  $U_{in} = 0.89\text{m/s}$ , (e)  $U_{in} = 1.04\text{ m/s}$ , (f)  $U_{in} = 1.28\text{m/s}$ , and (g)  $U_{in} = 2.35\text{m/s}$

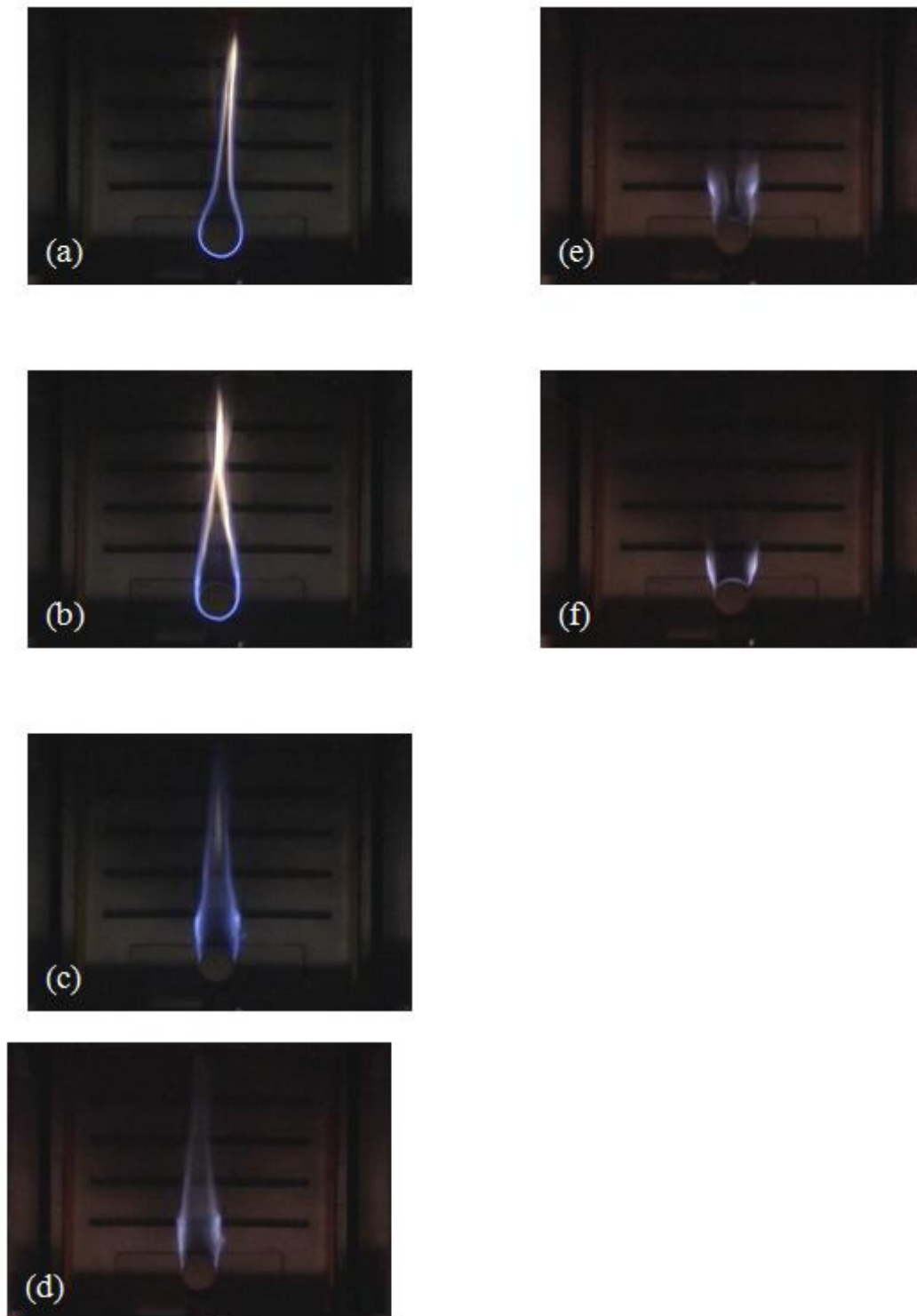
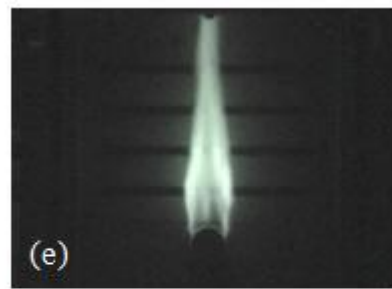
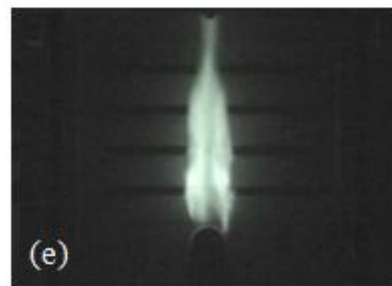
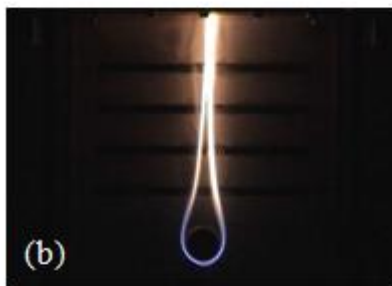


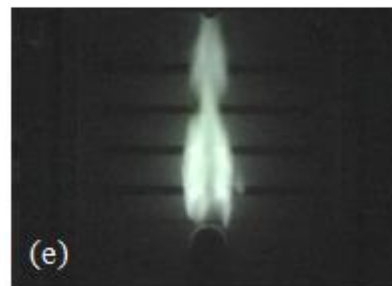
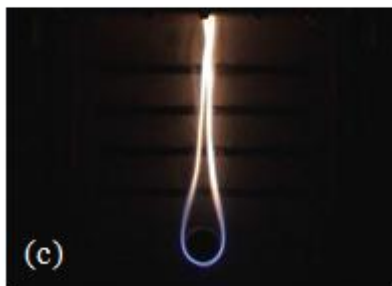
FIGURE 7 Series of flame configurations as a function of inflow velocity ( $v_w = 2.46\text{cm/s}$  and  $S=180^\circ$ ), (a)  $U_{in} = 0.41\text{m/s}$ , (b)  $U_{in} = 1.00\text{m/s}$ , (c)  $U_{in} = 1.2\text{m/s}$ , (d)  $U_{in} = 1.25\text{m/s}$ , (e)  $U_{in} = 1.58\text{m/s}$ , and (f)  $U_{in} = 3.10\text{m/s}$



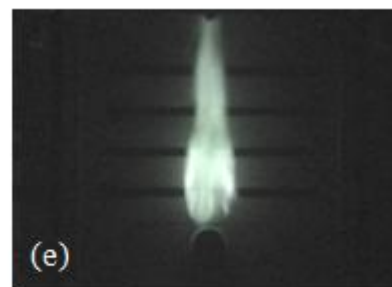
(1)  $t = 0$  sec



(2)  $t = 4$  ms



(3)  $t = 7$  ms



(4)  $t = 11$  ms

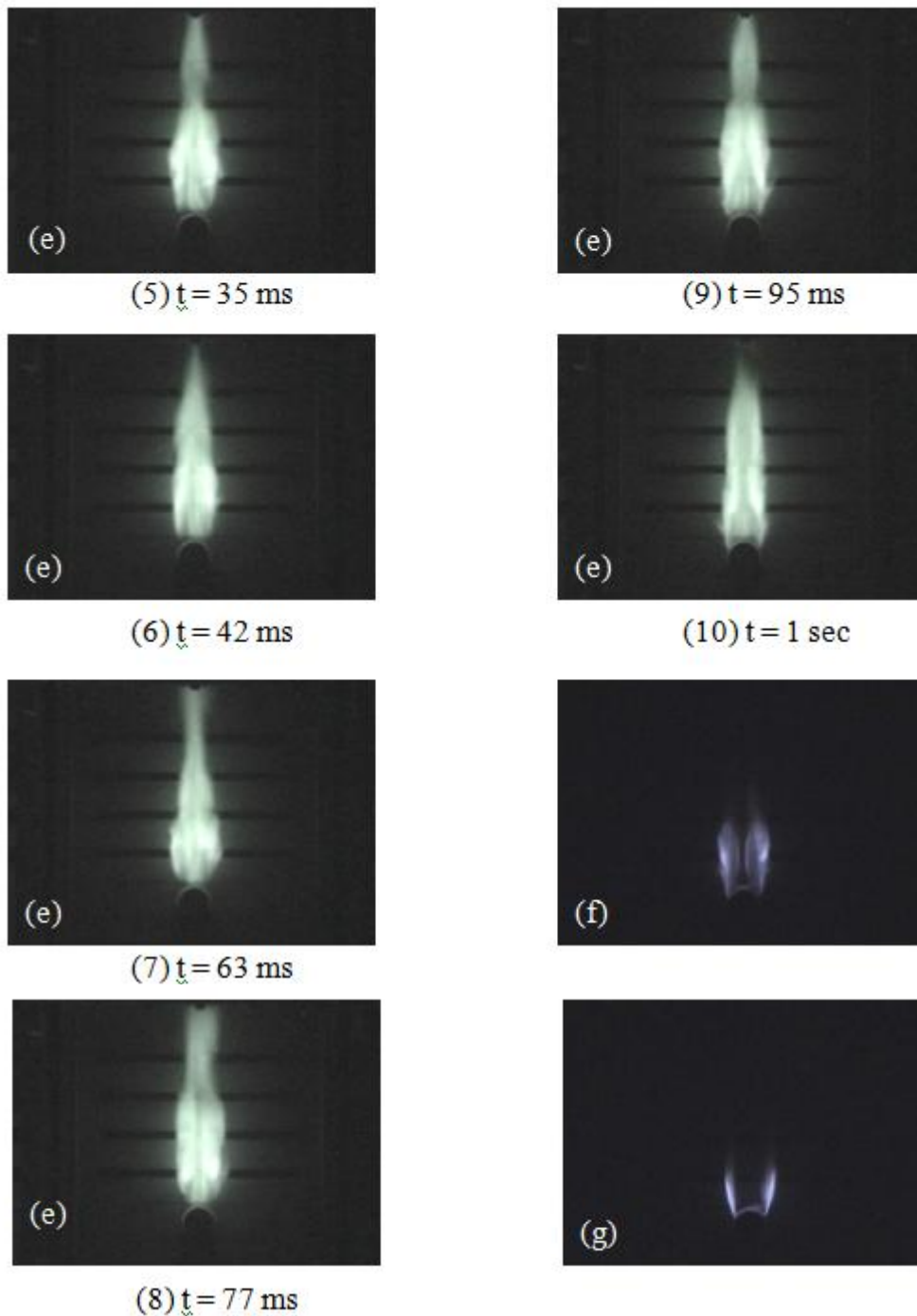


FIGURE 8 Series of flame configurations as a function of inflow velocity ( $v_w = 3.02\text{cm/s}$  and  $S = 180^\circ$ ), (a)  $U_{in} = 0.41\text{m/s}$ , (b)  $U_{in} = 0.62\text{m/s}$ , (c)  $U_{in} = 0.71\text{m/s}$ , (d)  $U_{in} = 1.00\text{m/s}$ , (e)  $U_{in} = 1.39\text{m/s}$  (Night shot photos), (f)  $U_{in} = 1.43\text{m/s}$ , and (g)  $U_{in} = 3.00\text{m/s}$

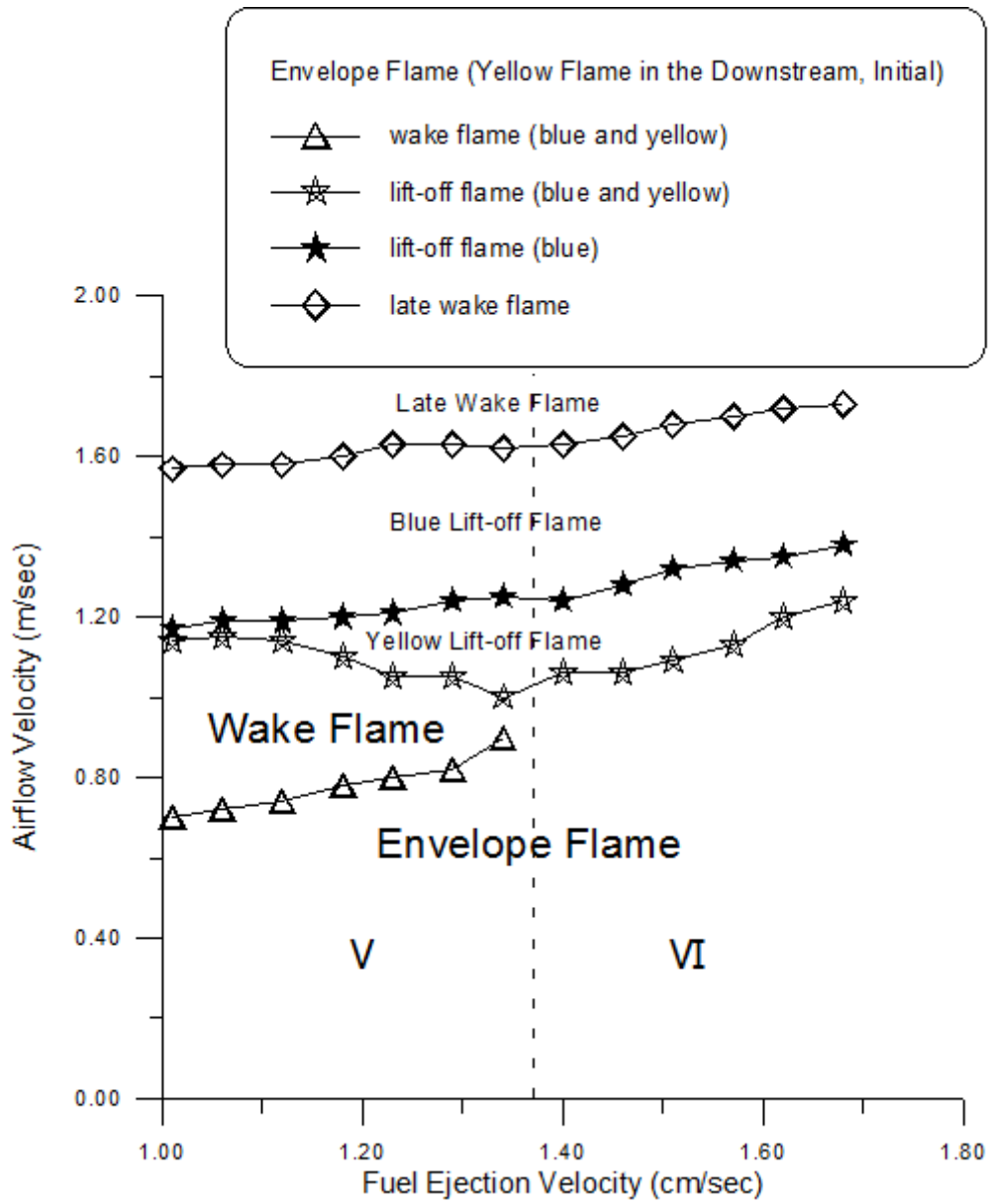
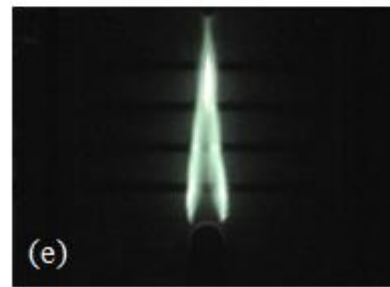
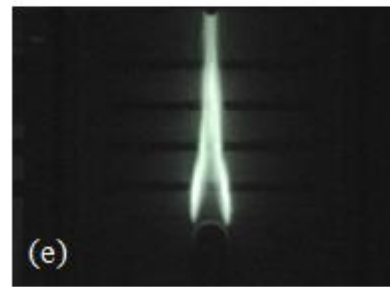


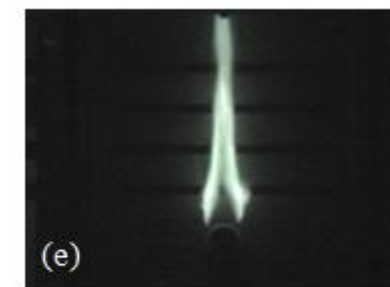
FIGURE 9 Various flame stabilization regions over a burner ( $S=360^\circ$ )



(1)  $t = 0$  sec



(2)  $t = 4$  ms



(3)  $t = 28$  ms

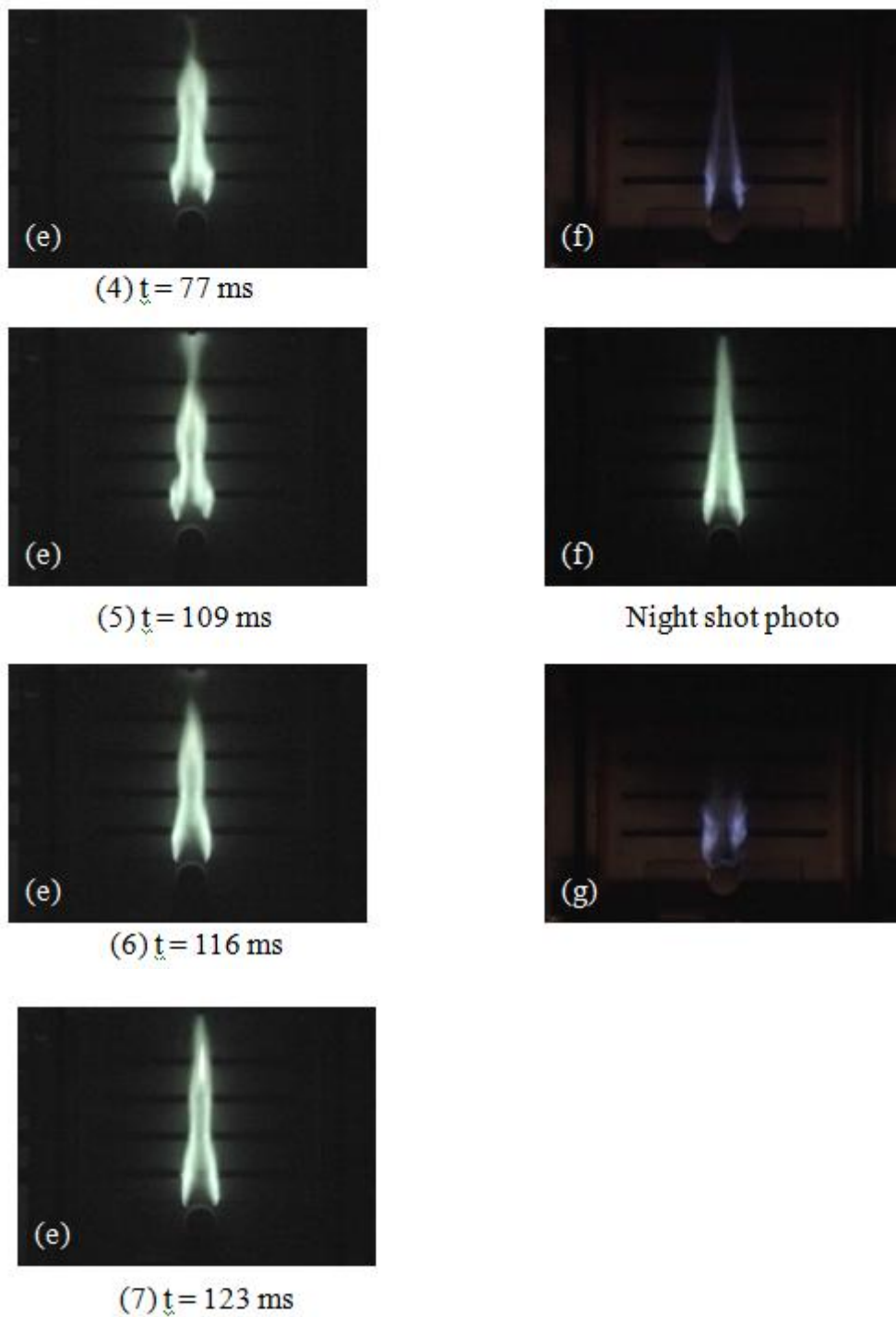


FIGURE 10 Series of flame configurations as a function of inflow velocity ( $v_w = 1.23\text{cm/s}$  and  $S=360^\circ$ ), (a)  $U_{in} = 0.41\text{m/s}$ , (b)  $U_{in} = 0.51\text{m/s}$ , (c)  $U_{in} = 0.80\text{m/s}$ , (d)  $U_{in} = 1.00\text{m/s}$ , (e)  $U_{in} = 1.05\text{m/s}$  (Night shot photos), (f)  $U_{in} = 1.21\text{m/s}$  and, (g)  $U_{in} = 1.63\text{m/s}$

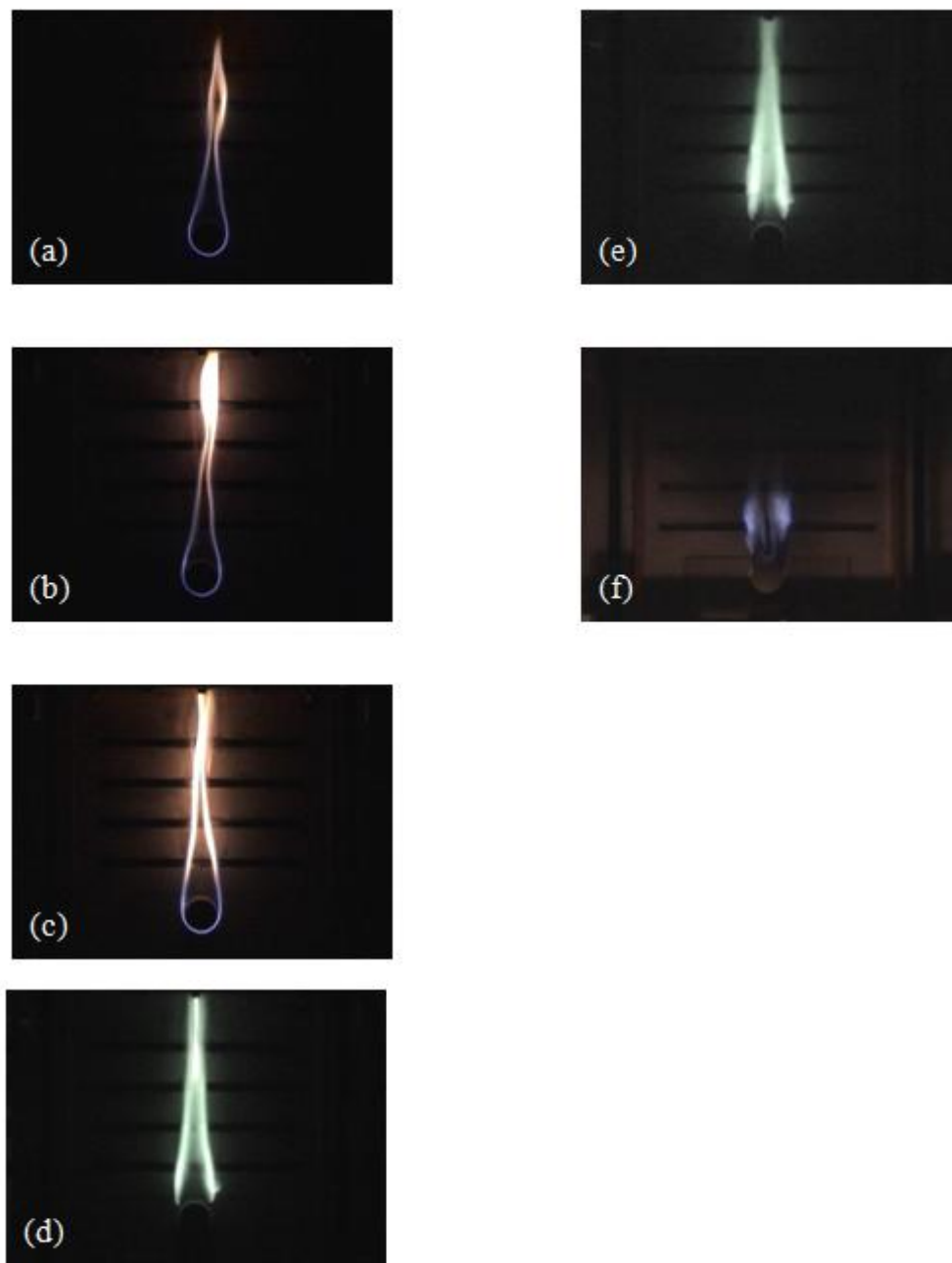


FIGURE 11 Series of flame configurations as a function of inflow velocity ( $v_w = 1.4\text{cm/s}$  and  $S=360^\circ$ ), (a)  $U_{in} = 0.41\text{m/s}$ , (b)  $U_{in} = 0.51\text{m/s}$ , (c)  $U_{in} = 0.84\text{m/s}$ , (d)  $U_{in} = 1.06\text{m/s}$  (Night shot photo), (e)  $U_{in} = 1.24\text{m/s}$  (Night shot photo), and (f)  $U_{in} = 1.63\text{m/s}$